SUGISAKA MASANORI

Journal of Advances in Artificial Life Robotics
Vol. 3(4); March (2023), pp. 185–192
ON LINE ISSN 2435-8061; ISSN-L 2435-8061
https://alife-robotics.org/jallr.html

Research Article

A Nonlinear Oscillator Coupling Model to Provide the Hough Transform Function Without the Discrete Voting Procedure

Amarbold Purev, Hiroaki Wagatsuma
Graduate School of Life Science and Systems Engineering, Kyushu Institute of Technology, 2-4 Hibikino, Wakamatsu, Kitakyushu 808-0196, Japan

ARTICLE INFO

Article History

Received 25 November 2022
Accepted 26 April 2023

Keywords

Hough transform
Line detection
Nonlinear dynamics
Coupled nonlinear oscillators
Kuramoto model

ABSTRACT

The most common algorithm for detecting straight lines in a digital image is the Hough Transform method. The method involves two consecutive steps: transforming the image edge location onto parameter space and voting procedure to acquire line characteristics. The former deals in continuous space, and the latter counts votes in a discrete matrix, making the algorithm sensitive to noise. We transformed each image pixel location to the parameter space as a Hough line and generated a nonlinear oscillator to attract them into the intersection with other lines. This concept could contribute to a line detection problem in image processing using a consistent mathematical description.

1. Introduction

Detecting lines in the image is crucial in computer vision [1], [2], [3] since it lays the foundation for object detection [4]. A common way to solve the problem is the Hough Transform (HT), mathematically sounds for detecting a unique focal point by projecting several line elements to the parameter space. HT projects the image data points from continuous spaces such as Cartesian to polar coordinate systems, while it requires the focal point search in discrete grids by voting. This voting process provides a trade-off problem, affecting the noise removal depending on the resolution. It needs higher resolution grids to achieve higher precision which needs more computational time. To overcome this limitation, we proposed a mathematical model based on the continuous space dynamics instead of the voting process. It is known as nonlinear dynamics having attractor dynamics. Based on ordinary differential equations, these dynamics can be simulated in a computer using numerical integration methods, such as the Euler and Runge-Kutta methods. A new method of combining the dual space projection in standard HT and a synchronization of self-organizing points to represent a single straight line based on the nonlinear dynamics could solve the original HT's drawbacks.

This paper focused on the mathematical solution for detecting straight lines, which can be obtained from nonlinear oscillator dynamics that produces synchronization phenomena in a limit cycle and the projection space of HT. Moving points can automatically concentrate on finding the intersection points of lines in the projection space. Therefore, there is no need for the voting process. Section 2 described the projection method from the Cartesian coordinate system to the parameter space and its algorithm for computer simulations. A typical nonlinear oscillator dynamic to replace the voting process was described in Section 3. In Section 4, we newly formulated the proposed system as a noise-resistant line detection method, followed by computer simulation results in Section 5 and a conclusion in Section 6.

2. Traditional Hough Transform Method

A technique for detecting shapes in an image using image analysis is the Hough Transform (HT) [5]. Paul Hough introduced this method in 1962, which has been applied in various fields [6], [7], [8]. HT converts the

Corresponding author's E-mail: purev.amarbold118@mail.kyutech.jp, waga@brain.kyutech.ac.jp

location of image points from Cartesian coordinates to a more concise representation in parameter space [9].

$$\rho = x\cos(\theta) + y\sin(\theta) \quad (1)$$

The location of points in the XY plane is transformed into parameter space by Eq. (1). As a result, each point in the XY plane becomes a sine curve. The length from the origin ρ and the angle θ, a line perpendicular to the line passing through edge points, are obtained by the intersection of these sine curves. Figure 1 showed this transformation.

HT method provides an accumulation array of zero values with $R \times T$ size to detect the intersection of edge points in Figure 1(b). R is the number of rows for the ρ value, and T is the number of columns for the θ value. The ρ value for every point is computed for every θ value, and the nearest ρ value in the accumulation array is increase by 1. This procedure is known as the voting procedure of HT. After going through all columns of the accumulation array, the cell with the maximum points describes the features of the perpendicular line. This transformation makes it possible to simplify the shape detection problem to a peak detection problem in parameter space.

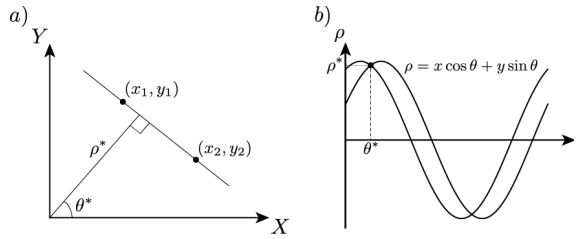

Fig. 1 Hough transformation. a) Points $(\boldsymbol{x_1}, \boldsymbol{y_1})$ and $(\boldsymbol{x_2}, \boldsymbol{y_2})$, a line with length $\boldsymbol{\rho}^*$ and angle $\boldsymbol{\theta}^*$ that is perpendicular to them in image space. b) Points transformed into sine curves in parameter space.

The HT method has the key benefit of being simple, enabling parallel information processing. This makes the method resistant to noise and capable of detecting partially hidden or distorted shapes. In addition, the method could be set up to detect a fixed number of shapes in an image.

However, the HT method's simplicity becomes a drawback when detecting shapes other than straight lines. The amount of computations grows as the number of parameters required to define the shape grows [10], [11]. For instance, detecting a circle in an image would need a three-dimensional accumulation array for the circle's center (x, y) and its radius r. With respect to efforts of researchers to enhance the HT method's efficiency through software optimization [12], [13], [14], [15]. specialized hardware [16], and the use of artificial intelligence [17], this problem still remains unsolved.

By using an accumulation array in the system, HT cannot avoid difficulties, such as the array's size determination to adjust for precise detection. The method becomes inaccurate if the grid size of the array is too large to discriminate the true spot, and the computational time becomes costly if the grid size is too small in an unnecessary manner. Furthermore, HT only detects lines that have infinite lengths. This is because HT uses its parameters to represent lines that do not contain information about the line length. Therefore, the HT cannot detect lines that have finite lengths.

3. Coupled Nonlinear Oscillator Dynamics

3.1. *Synchronization of Kuramoto Model*

The Kuramoto model (KM) is a mathematical model investigating oscillator synchronization [18]. It is frequently used in areas such as physics [19], [20]. biology [21], and chemistry and has been utilized in various contexts, such as neurophysiology [22], [23], distributed power generation [24], [25], and secure communication [26], [27]. In this paper, we suggest using modified model of KM to cluster edges in images based on their collinearity.

The following equation describes the standard model of the KM

$$\dot{\varphi}_i = \omega_i + \frac{K}{N}\sum_{j=1}^{N}\sin(\theta_j - \theta_i). \quad (2)$$

Eq. (2) represents a group of N oscillators with a limit cycle. These oscillators have natural frequencies ω_i and phases θ. The coupling constant K, and the coupling between oscillators is determined by the sine of the difference in their phases. The phases change over time according to first-order dynamics.

The KM is not commonly used in image processing because oscillators are dynamic while image edges are static. However, in [28], researchers applied it to segment color images. Using a coupled network, they provided three oscillating curves for the red, green, and blue pixel values of color images. This produced a superposition of oscillation for the image pixels.

It suggests that the KM's attractor dynamics of coupled nonlinear oscillators changes edge coordinates from discrete to continuous space. This function will enable the clusterization of edges in parameter space with the KM, removing the necessity for an accumulation array in the standard HT method.

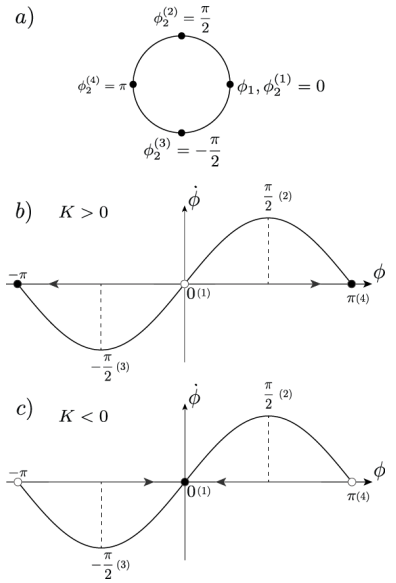

Fig. 2 Interaction between two nonlinear oscillators $\boldsymbol{\varphi_1}$and $\boldsymbol{\varphi_2}$. The initial positions are shown in a). The behavior of the second oscillator is shown in b) when $\boldsymbol{K > 0}$ and c) when $\boldsymbol{K < 0}$. A black dot indicates a stable point, and a white dot indicates an unstable point.

In order to analyze how the KM can detect lines in images, we must first examine the behavior of straightforward systems. By understanding their behavior, it leads a model to classify image edges based on their collinearity accurately.

3.2. *Analysis of Stability for two Coupled Nonlinear Oscillators*

Let us assume that a system with two oscillators, $\dot{\varphi}_1$ and $\dot{\varphi}_2$, that behaves according to

$$\begin{cases} \dot{\varphi}_1 = 0 \\ \dot{\varphi}_2 = K \sin(\varphi_2 - \varphi_1) \end{cases} \tag{3}$$

The starting conditions are $\varphi_i(0) = \varphi_i^0$, where φ is the phase of the ith oscillator and K is the coupling strength.

To simplify the analysis, it is assumed that $\dot{\varphi}_1$ is always equal to 0 and focused on the dynamics of the second oscillator. The initial values of $\varphi_2^{(n)} = [0, \pi/2, -\pi/2, \pi], n = 1 \ldots 4$, as shown in Figure 2.

The description gives the definition of phase synchronization as follows.

Definition 1. Let $\{\boldsymbol{\varphi_i(t)}\}_{\boldsymbol{i=1}}^{\boldsymbol{2}}$ be solution of our system. The oscillators converge to phase synchronization if

$$\lim_{t\to\infty} \left|\varphi_i(t) - \varphi_j(t)\right| = 0, \quad \text{for } i \neq j. \tag{4}$$

Let us examine how our system behaves according to Eq. (3) when applying different initial conditions.

Example 1. $\varphi_1(0), \varphi_2(0) = 0$

The solution to the equation is $\varphi_1(t) = 0$ and $\varphi_2(t) = 0$. This means that there is phase synchronization.

Example 2. $\varphi_1(0) = 0, \varphi_2(0) = \frac{\pi}{2}, K > 0$

$$\begin{aligned} \varphi_2(t) &= K \sin\left(\frac{\pi}{2} - 0\right) \\ &= K \sin\left(\frac{\pi}{2}\right) \\ &= K \end{aligned} \tag{5}$$

Because $K > 0$, $\dot{\varphi}_2(t) \to \pi$ and the second oscillator converges to the anti-phase.

Example 3. $\varphi_1(0) = 0, \varphi_2(0) = -\frac{\pi}{2}, K > 0$

$$\begin{aligned} \varphi_2(t) &= K \sin\left(-\frac{\pi}{2} - 0\right) \\ &= K \sin\left(-\frac{\pi}{2}\right) \\ &= -K. \end{aligned} \tag{6}$$

Because $\dot{\varphi}_2(t) < 0$, $\dot{\varphi}_1(t) \to -\pi$ the second oscillator converges to the anti-phase as well.

Example 4. $\varphi_1(0) = 0, \varphi_2(0) = \pi, K > 0$

$$\begin{aligned} \varphi_2(t) &= K \sin(\pi - 0) \\ &= K \sin(\pi) \\ &= 0 \end{aligned} \tag{7}$$

When the initial position of $\varphi_2(0) = \pi$ and $\varphi_2(t) = 0$, the second oscillator starts at the anti-phase stable point of π and does not move as $t \to \infty$.

Although both oscillators converge in Example 1, the 0 point is unstable as shown in Examples 2, 3. 4. As a result, the system described by Eq. (3) converges to the anti-phase. But, if the coupling strength is negative, the two oscillators will converge after performing the same calculations as in the previous examples.

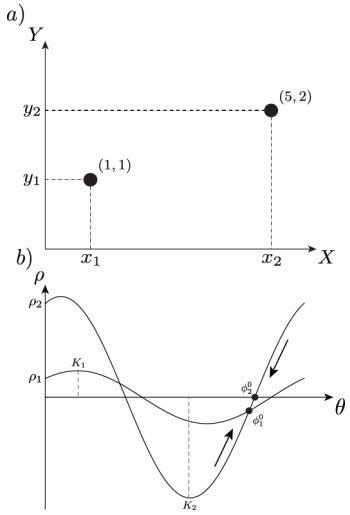

Fig. 3 Example of points (1,1) and (5,2). a) Image space. b) Hough space.

4. Coupled Nonlinear Oscillator-based Hough Transform for Noise-Robust Line Detection

4.1. *Coupled Nonlinear Oscillator-based Hough Transform with single attractor*

The standard HT method is explained in Section 1. Instead of the standard HT voting scheme, a model can be considered by eliminating it with a nonlinear system of equations as the proposed model. Each point in the image space is considered as a separate nonlinear oscillator and coupled together using the following system of equations

$$\begin{cases} \dot{\varphi}_1 = 0 \\ \dot{\varphi}_2 = \dfrac{\rho_1 - \rho_2}{K^2} + (\varphi_1 - \varphi_2) \end{cases} \tag{8}$$

The initial conditions $\varphi_i(0) = \varphi_i^0$, where φ is the phase of the ith oscillator, ρ is the amplitude of Hough line at the φ phase and K is the coupling strength based on the maximum amplitude of the ρ value.

For the sake of finding where both points meet in the Hough space, the ρ and θ values of each oscillator have to take exact same values individually. According to Eq. (3), it implies that φ_1 stops and then φ_2 moves towards φ_1. Thus, the first oscillator will pull the second one to itself.

Consequently, choosing the initial phase of the first oscillator at the intersection of Hough lines is essential and can be calculated analytically

$$\begin{gathered} \rho_1 = \rho_2 \\ x_1 \cos\theta + y_1 \sin\theta = x_2 \cos\theta + y_2 \sin\theta \\ \theta = \tan^{-1}(-(x_1 - x_2)/(y_1 - y_2)). \end{gathered} \tag{9}$$

When the starting phase of the first oscillator as $\varphi_1^0 = \tan^{-1}(-(x_1 - x_2)/(y_1 - y_2))$, it goes where two Hough lines intersect and start the second oscillator at the fixed point, where $\rho_2 = 0$. In Eq. (9) to get the $\theta = \tan^{-1}(-x_2/y_2)$, $\varphi_2^0 = \tan^{-1}(-x_2/y_2)$, the coupling strength K is the highest ρ value for each Hough line, which is $K_i = x_i^2 + y_i^2$.

Nevertheless, it faces another problem to change the sign to refrain from the anti-phase synchronization problem in Section 3.2.

Example 5 showed how to solve this problem.

Example 5. Two points, $p_1 = (x_1, y_1) = (1,1)$ and $p_2 = (x_2, y_2) = (5,2)$ are given in the image space, as shown in Figure 3. For finding the initial values, two oscillators need to converge with the same coupling as Eq. (9). $\varphi_1^0 = \tan^{-1}(-(x_1 - x_2)/(y_1 - y_2)) = 4.9574$ rad, $\varphi_2^0 = \tan^{-1}(-x_2/y_2) = 5.0929$ rad, $K_2 = x_2^2 + y_2^2 = 29$.

Figure 3 showed φ_i^0 has 2 solutions for each oscillator in a 2π period. Therefore, our model needs to be able to change the sign depending on where the initial phase of the oscillator is. This provides a function to find the direction of the oscillator by getting the slope of the second Hough line from the first derivative of ρ function

$$\frac{d\rho}{d\theta} = y\cos\theta - x\cos\theta. \tag{10}$$

Ultimately there can only be four distinct cases:

(i) $\varphi_1^0 > \varphi_2^0,\ \rho_2'(\varphi_2^0) > 0$
(ii) $\varphi_1^0 < \varphi_2^0,\ \rho_2'(\varphi_2^0) < 0$
(iii) $\varphi_1^0 > \varphi_2^0,\ \rho_2'(\varphi_2^0) < 0$
(iv) $\varphi_1^0 < \varphi_2^0,\ \rho_2'(\varphi_2^0) > 0$

By examining the options, four different groups were defined into two categories, (i, ii) and (iii, iv), with the identical effect. Then Eq. (8) changes into the following system of equations

$$\begin{cases} \dot{\varphi}_1 = 0 \\ \dot{\varphi}_2 = \dfrac{\rho_1 - \rho_2}{K^2} + (\varphi_1 - \varphi_2), & \text{if A or B} \\ \dot{\varphi}_2 = \dfrac{\rho_2 - \rho_1}{K^2} + (\varphi_1 - \varphi_2), & \text{if C or D} \end{cases} \tag{11}$$

where $A = (\varphi_1^0 > \varphi_2^0, \varphi_2'(\varphi_2^0) < 0)$, $B = (\varphi_1^0 < \varphi_2^0, \rho_2'(\varphi_2^0) > 0)$, $C = (\varphi_1^0 > \varphi_2^0, \rho_2'(\varphi_2^0) > 0)$, $D = (\varphi_1^0 < \varphi_2^0, \rho_2'(\varphi_2^0) < 0)$.

4.2. *Proposed Model for Pair-wise Coupling*

The previous model in Eq. (11) has a significant disadvantage in real-life scenarios. Because to analyze an image in full, the algorithm has to run N times for all the edge points, selecting a single edge point as an attractor in each loop. Therefore, the pair-wise coupling is better from an optimization standpoint, where two oscillators attract each other at the same converging at the intersection of Hough line

$$\dot{\varphi}_i = \begin{cases} \frac{\rho_j - \rho_i}{K_i} + (\varphi_j - \varphi_i), & \text{if A or B} \\ -\frac{\rho_j - \rho_i}{K_i} + (\varphi_j - \varphi_i), & \text{otherwise} \end{cases} \quad (12)$$

where i, j – is the index of first and second oscillator in pair-wise coupling.

The only difference from Eq. (11) other than pair-wise coupling, the initial phase of all oscillators φ_i^0 will be at the θ-axis in parameter space, which means

$$\begin{aligned} x_i \cos\varphi_i + y_i \sin\varphi_i &= 0 \\ x_i \cos\varphi_i &= -y_i \sin\varphi_i \\ \frac{\sin\varphi_i}{\cos\varphi_i} &= \left(-\frac{x_i}{y_i}\right) \\ \varphi_i &= \tan^{-1}\left(-\frac{x_i}{y_i}\right) \end{aligned} \quad (13)$$

The above condition ensures that the oscillators will have uniform behavior and derivative in Eq. (10) will never have a 0 value at the start.

A detailed description of the coupled nonlinear oscillator-based HT algorithm and the traditional HT method is given in [29].

5. Results and Discussion

The following section shows the proposed algorithm's results for pair-wise coupling on various setups and evaluates the accuracy and error of detection.

5.1. *Proposed Model for Pair-wise Coupling*

The proposed model in Eq. (12) was tested extensively in various situations. Figure 4 shows the experiment setup: only line points (a-d), line points with noise (e), distorted line points with noise (f), grid structure (g), and varying image size (h).

First, for only line points experiment, four experiments were conducted for each type of line with only line points. The number of line points $N_{line} = 100$, and the of iterations up to $iter < 20000$ was selected. The proposed model initiated a list of all points in the image., then extracted two random points from the list, and synchronized them until no points were left.

Then, for line points with noise, random noise points were added to the lines in the previous experiment. This experiment was conducted 20 times for each type of line, a total of 80 experiments. Sample figures of each line type are shown in Figure 5. Since pair-wise coupling selects two random points out of all points, including line and noise, all of the line points are not detected.

Additionally, a scenario with the distorted line in the presence of noise was tested (Figure 4(f)). In this scenario the proposed model struggles to distinguish between line and noise points, because oscillators converge to the absolute theoretical straight line. However, a distorted line is theoretically not a single line but multiple lines. As a result, the number of line points is significantly decreased compared to the previous experiments, which makes it harder to detect line points.

Furthermore, a grid structure was tested to evaluate the proposed model's ability to detect multiple lines, with and without noise. When no noise points are present in the image, pair-wise coupling performs well. However, if the noise points disrupt the image, the model fails to provide good results.

Lastly, the convergence rate based on points distance was tested. In this experiment, 20 evenly distributed points from 2 to 1000 were converged together and the number of iterations for convergence was registered. Figure 6 shows the ratio between Euclidean distance and convergence rate. The analysis shows the convergence speed of oscillators based on their Euclidean distance $= \sqrt{(x_1 - x_2)^2 + (y_1 - y_2)^2}$ in image space with $\Delta e = 10^{-6}$ precision. As shown in the graph, when the D is close to 0, it takes a significant number of iterations to converge. However, the number of iterations quickly drops to 100 when $D > 30$. A slight difference in D means the difference ρ is also insignificant, which affects the oscillator's speed to be slow.

Table 1 shows the average line detection rates (%) for line types in above described experiments. The pair-wise coupling has high detection rates with high precision thresholds.

6. Conclusion

Our mathematical formulation and computer experiment clearly demonstrated the replacement of the HT voting scheme by coupled nonlinear oscillator dynamics. We analyzed single attractor model to understand oscillator behavior in simple cases and it was successfully extended to the pair-wise model to improve limitations on previous model. The model was experimentally tested in different possible straight-line

configurations. The pair-wise coupling method shows high accuracy and precision.

By using coupled nonlinear oscillators, replacing the accumulation array was achieved and the desired precision can automatically be set in the proposed model. In future work, performance improvement in real-time applications will be developed based on the proposed model. applications will be developed based on the proposed model.

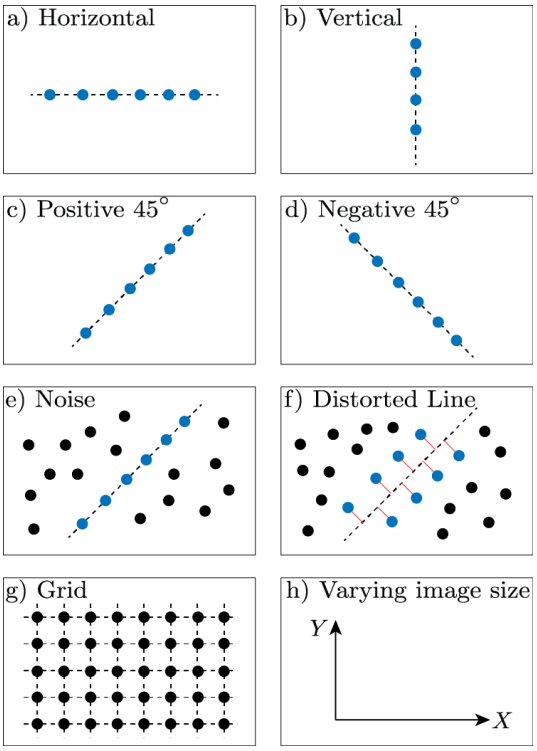

Fig. 4 Scope of the experiment on pair-wise coupling model. a) – d) represents different types of straight lines with line points only. e) – f) represents straight line points in different scenarios. Blue points are the straight line points, whereas black ones are noise points.

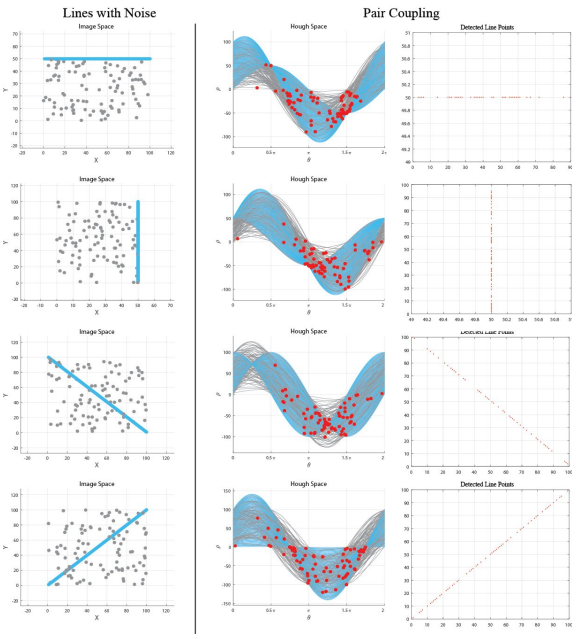

Fig. 5 Single line points in a noisy environment with their Hough space and detected line points using pair-wise coupling. Blue dots in image space and blue lines in hough space are line points, whereas gray dots and gray lines correspond to noise. Red dots in Hough space are individual oscillators.

Table 1. Line point detection rate based on the set precision for pair-wise coupling of oscillators.

Line Types	Precision (ε)	Line Ratio (%)
Single Line	10^{-6}	99.75
Line and Noise	10^{-13}	40.49
Distorted Line and Noise	10^{-12}	81.71
Grid Line	10^{-7}	95.00
Grid Line and Noise	10^{-12}	76.13
Varying Image Size	10^{-10}	99.10

Acknowledgements

This work was supported in part by JSPS KAKENHI (16H01616, 17H06383), Project on Regional Revitalization Through Advanced Robotics (Kyushu Institute of Technology/Kitakyushu city, Japan) and the

New Energy and Industrial Technology Development Organization (NEDO).

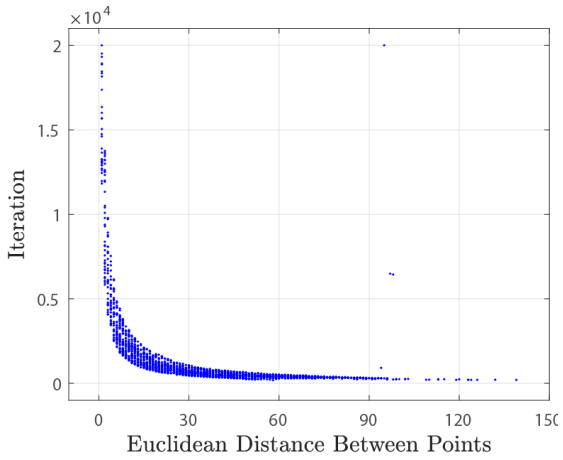

Fig. 6 Pair-wise coupling convergence rates based on the Euclidean distance $\boldsymbol{D}$ between points $\boldsymbol{p_1} = (\boldsymbol{x_1}, \boldsymbol{y_1})$ and $\boldsymbol{p_2} = (\boldsymbol{x_2}, \boldsymbol{y_2})$.

References

1. B. K. P. Horn, "Robot Vision", MIT Press, 1986.
2. W. Chen, W. Wang, K. Wang, Z. Li, H. Li, S. Liu, "Lane departure warning systems and lane line detection methods based on image processing and semantic segmentation: A review", JTTE (English Edition), Vol. 7, No. 6, pp. 748-774, 2020.
3. Q. Luo, X. Fang, L. Liu, C. Yang, Y. Sun, "Automated Visual Defect Detection for Flat Steel Surface: A Survey", IEEE Transactions on Instrumentation and Measurement, Vol. 69, No. 3, pp. 626-644, 2020.
4. Q. -R. Wei, D. -Z. Feng, W. Zeng, J. -B Zheng, "Rapid line-extraction method for SAR images based on edge-field features", IEEE Geoscience and Remote Sensing Letters", Vol. 14, No. 10, pp. 1865-1869, 2017.
5. P. V. C. Hough, "Method and means for recognizing patterns", US Patent 3069654A, 1962.
6. T. K. Greeshma, S. Priya, C. Chaithanya, "A Survey on Line Detection Techniques using Different Types of Digital Images", IJARCET, Vol. 8, No. 5, pp. 162-168, 2019.
7. F. Tschopp, C. von Einem, A. Cramariuc, D. Hug, A. W. Palmer, R. Siegwart, M. Chli, J. Nieto, "Hough^{2}Map – Iterative Event-Based Hough Transform for High-Speed Railway Mapping", IEEE Robotics and Automation Letters, Vol. 6, No. 2, pp. 2745-2752, 2021.
8. C. Dalitz, T. Schramke, M. Jeltsch, "Iterative Hough Transform for Line Detection in 3D Point Clouds", Image Processing On Line, Vol. 7, pp. 184-196, 2017.
9. R. O. Duda, P. E. Hart, "Use of the Hough Transformation to Detect Lines and Curves in Pictures", Communications of the ACM, Vol. 15, No. 1, pp. 11-15, 1972.
10. D. H. Ballard, "Generalizing the Hough transform to detect arbitrary shapes, Pattern Recognition, Vol. 13, No. 2, pp. 111-122, 1981.
11. N. Kiryati, Y. Eldar, A. M. Bruckstein, "A Probabilistic Hough Transform", Pattern Recognition, Vol. 24, No. 4, pp. 303-316, 1991.
12. L. A. F. Fernandes, M. M. Oliveira, "Real-time line detection through an improved Hough Transform voting scheme", Pattern Recognition, Vol. 41, No. 1, pp. 299-314, 2008.
13. H. F. Li, D. Pao, R. Jayakumar, "Improvements and Systolic Implementation of the Hough Transformation for straight line detection", Pattern Recognition, Vol. 22, No.6, pp. 697-706, 1989.
14. S. Du, B. J. van Wyk, C. Tu, X. Zhang, "An improved Hough transform neighborhood map for straight line segments", IEEE Transactions on Image Processing, Vol. 19, No.3, pp. 573-585, 2010.
15. N. Aggarwal, W. C. Karl, "Line detection in images through regularized Hough transform", IEEE Transactions on Image Processing, Vol. 15, No. 3, pp. 582-591, 2006.
16. E. Hajjouji, S. Mars, Z. Asrih, A. E. Mourabit, "A novel FPGA implementation of Hough Transform for straight lane detection", JESTECH, Vol. 23, No. 2, pp. 274-280, 2020.
17. M. W. Spratling, "A neural implementation of the Hough transform and the advantages of explaining away", Image and Vision Computing, Vol. 52, No. 1, pp. 15-24, 2016.
18. J. A. Acebron, L. L. Bonilla, C. J. P. Vicente, F. Ritort, R. Spigler, "The Kuramoto model: A simple paradigm for synchronization phenomena", Reviews of Modern Physics, Vol. 77, No. 1, pp. 137-185, 2005.
19. M. Ignatov, M. Ziegler, M. Hansen, H. Kohlstedt, "Memristive stochastic plasticity enables mimicking of neural synchrony: Memristive circuit emulates an optical illusion", Science Advances, Vol. 3, No. 10, pp. e1700849, 2017.
20. M. Ignatov, M. Hansen, M. Ziegler, H. Kohlstedt, "Synchronization of two memristively coupled van der Pol oscillators", Applied Physics Letters, Vol. 108, No. 8, pp. 084105, 2016.
21. H. Mizuhara, Y. Yamaguchi, "Human cortical circuits for central executive function emerge by theta phase synchronization", NeuroImage, Vol. 36, No. 1, pp. 232-244, 2007.
22. T. Cattai, S. Colonnese, M. C. Corsi, D. S. Bassett, G. Scarano, F. D. V. Fallani, "Phase/amplitude synchronization of brain signals during motor imagery BCI tasks", arXiv:1912.02745 [q-bio.NC], 2019.
23. V. Rohr, R. Berner, E. L. Lameu, O. V. Popovych, S. Yanchuk, "Frequency cluster formation and slow oscillations in neural populations with plasticity", PLoS ONE, Vol. 14, No. 11, pp. e0225094, 2019.
24. P. A. Arinushkin, T. E. Vadivasova, "Nonlinear damping effects in a simplified power grid model based on coupled Kuramoto-like oscillators with inertia", Chaos, Solitons & Fractals, Vol. 152, No. 1, pp. 111343, 2021.
25. Y. Guo, D. Zhang, Z. Li, Q. Wang, D. Yu, "Overviews on the applications of the Kuramoto model in

modern power system analysis, International Journal of Electrical Power & Energy Systems, Vol. 129, pp. 106804, 2021.
26. A. Argyris, D. Syvridis, L. Larger, V. A. Lodi, P. Colet, I. Fischer, J. G. Ojalvo, C. R. Mirasso, L. Pesquera, K. A. Shore, “Chaos-based communications at high bit rates using commercial fibre-optic links”, Nature, Vol. 438, No. 7066, pp. 343-346, 2005.
27. P. Feketa, A. Schaum, T. Meurer, D. Michaelis, K. Ochs, “Synchronization of nonlinearly coupled networks of Chua oscillators”, IFAC-PapersOnLine, Vol. 52, No. 16, pp. 628-633, 2019.
28. X. Lu, Y. Qiao, X. Chen, J. Miao, L. Duan, “Color Image Segmentation Based on Modified Kuramoto Model”, Procedia Computer Science, Vol. 88, No. 1, pp. 245-258, 2016.
29. A. Purev, H. Wagatsuma, “Basic Concept of the Nonlinear Oscillator-Based Hough Transform Implementation to Improve the Voting Procedure in the Scheme of Continuous Dual Spaces”, ICAROB2023, 2023.

Authors Introduction

Mr. Amarbold Purev

He received his Master's degree from the School of Mechanical Engineering and Transportation, Mongolian University of Science and Technology, Mongolia in 2019. He is currently a Doctoral course student in Kyushu Institute of Technology, Japan.

Dr. Hiroaki Wagatsuma

He received his M.S., and Ph.D. degrees from Tokyo Denki University, Japan, in 1997 and 2005, respectively. In 2009, he joined Kyushu Institute of Technology, where he is currently Professor of the Department of Human Intelligence Systems. His research interests include nonlinear dynamics and robotics. He is a member of IEEE.